On the Distribution of Climate Change Resulting from an Increase in CO_2 Content of the Atmosphere

SYUKURO MANABE AND RICHARD T. WETHERALD

Geophysical Fluid Dynamics Laboratory/NOAA, Princeton University, Princeton, NJ 08540

ABSTRACT

A study of the climatic effect of doubling or quadrupling of CO_2 in the atmosphere has been continued by the use of a simple general circulation model with a limited computational domain, highly idealized geography, no seasonal variation of insolation, and a simplified interaction between cloud and radiative transfer.

The results from the numerical experiments reveal that the response of the model climate to an increase of CO_2 content in air is far from uniform geographically. For example, one can identify the high-latitude region of the continent where the runoff rate increases markedly, a zonal belt of decreasing soil moisture around 42° latitude, and a zone of enhanced wetness along the east coast of the subtropical portion of the model continent.

The general warming and the increase of moisture content of air, which results from a CO_2 increase, contributes to the large reduction of the meridional temperature gradient in the lower model troposphere because of 1) poleward retreat of highly reflective snow cover and 2) large increase in the poleward transport of latent heat. The reduction of the meridional temperature gradient appears to reduce not only the eddy kinetic energy, but also the variance of temperature in the lower model troposphere. The penetration of moisture into higher latitudes in the CO_2-rich warm climate is responsible for the large increase of the rates of precipitation and runoff in high latitudes of the model.

1. Introduction

The climatic effects of an increase in the CO_2 content of the atmosphere have been the subject of many investigations [see Schneider (1975) and Ramanathan and Coakley (1978) for comparative evaluations of these studies.] Manabe and Wetherald (1975, hereafter identified as MW75) investigated this problem by the use of a highly simplified model of the atmospheric general circulation. The simplified characteristics of the MW75 model included a limited computational domain with idealized geography, no seasonal variation, no heat transport by ocean currents and fixed cloudiness. Based on the results from this model, MW75 discussed the response of the zonal- and area-mean climates to the increase in the CO_2 content of the atmosphere. However, MW75 did not evaluate the geographical distribution of the response which, despite the idealization of geography mentioned above, reveals some interesting characteristics that deserve further investigation. Furthermore, it has been realized that the idealization of geography, owing to the simplicity of continental shape, facilitates the identification of the influences of a continent on the response of climate to external (or internal) stimuli. Therefore, it was decided to perform numerical experiments similar to that of MW75, after making some modifi-

cations to the model, to study the geographical character of the CO_2-induced climatic change.

After detailed analysis of the results from the present series of numerical experiments, it was noted that the poleward transport of latent heat plays an important role in determining the latitudinal distribution of the response of the model climate and deserves further discussion. Therefore, the sensitivity of the zonal-mean climate continues to receive a major emphasis in this study, even though it was one of the main topics covered in MW75.

One of the new features of the model used in the present study is the treatment of cloud cover. In the previous study (MW75), cloud cover was prescribed to vary only as a function of latitude and altitude, i.e., the cloud cover was zonally uniform. However, it is possible that the interaction between cloud cover and radiative transfer may significantly influence the distribution of the climatic response to the increase in CO_2 content of the atmosphere. Therefore, a highly simplified scheme of cloud prediction is incorporated into the present model.

Another important difference between the previous and present models is the poleward extent of the computational domain. In the MW75 model, the poleward boundary was placed at the 81.7° latitude circle because of the use of a Mercator map coordinate, whereas in the present model, the
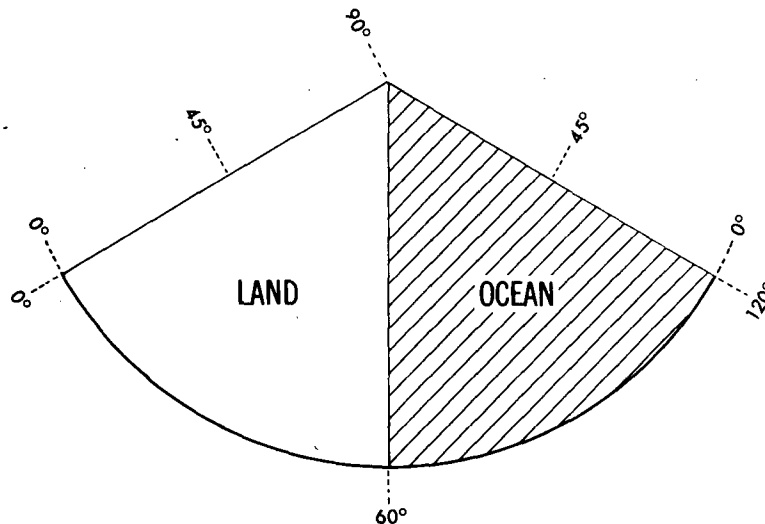
FIG. 1. Land-ocean distribution of the model.

computational domain extends to the pole. It is possible that this difference in the computational domain has some influence on the behavior of the snow cover in high latitudes.

Obviously, because of the many simplifications and idealizations of the model, the quantitative details of this study should be interpreted with caution. It is hoped, however, that this study yields some preliminary insight on the distribution of the possible climatic response to the increase of atmospheric carbon dioxide, and that it establishes a foundation for a similar study of this problem with a global climate model having realistic geography.

2. Model structure

The model includes prognostic equations for the horizontal wind velocity, surface pressure, temperature and water vapor mixing ratio, which are written in finite-difference form on a spherical coordinate system. The governing equations are the momentum equations, mass continuity equation, thermodynamical energy equation and the water vapor continuity equation. With the hydrostatic approximation, the momentum equation explicitly computes the rate of velocity change due to the momentum exchange by the large-scale flow and the Coriolis and pressure gradient forces. In addition, this calculation includes the contributions of horizontal and vertical mixing due to subgrid-scale eddies as proposed by Smagorinsky et al. (1965). As suggested by Phillips (1957), the vertical coordinate is chosen to be sigma, i.e., pressure normalized by surface pressure. The thermodynamic energy equation computes the rate of temperature change due to the three-dimensional advection of temperature by the large-scale flow, adiabatic compression and expan-

sion, radiative transfer, horizontal and vertical mixing by subgrid-scale eddies, a dry and moist convective adjustment and the condensation of water vapor. The water vapor continuity equation predicts the rate of change of the water vapor mixing ratio due to the three-dimensional advection by the large-scale flow, horizontal and vertical mixing by subgrid-scale eddies, and the moist convective adjustment and nonconvective condensation as proposed by Manabe et al. (1965).

The numerical integration of the prognostic equations described above is carried out at nine vertically spaced finite-difference levels which are chosen to represent the lower stratosphere, the Ekman boundary layer and the troposphere. For the horizontal finite differencing, a regular latitude-longitude grid system with a meridional spacing of 4.5° and longitudinal spacing of 5.0° is used (for further details see Manabe et al., 1975).

The computational domain and geography of the model are shown in Fig. 1. An insulated free-slip wall is placed at the equator and cyclical continuity is assumed for the two meridional boundaries of the 120° longitude sector. The computational domain is divided into two equal areas of continent and "ocean." It should be stressed that this model does not include ocean dynamics. The "ocean" portion is simply considered to be an area possessing an infinite supply of moisture for evaporation. The model ocean resembles the actual ocean in the sense that it is wet, but it has no heat capacity and no heat transport by ocean currents.

The radiative transfer section of the model computes the transfer of solar and terrestrial radiation incorporating the effects of water vapor, carbon dioxide, ozone and clouds. The transfer of terrestrial radiation is computed by a method which was orig-

inally developed by Rogers and Walshaw (1966) and was modified by Stone and Manabe (1968). The method is significantly different from the version formulated by Manabe and Strickler (1964) which was used in MW75. The scheme for computing solar heating of the atmosphere is identical to that described by Manabe and Strickler (1964) and Manabe and Wetherald (1967). The distribution of water vapor is determined from the prognostic equation for water vapor. The mixing ratio of carbon dioxide is assumed to be uniform everywhere. A zonally uniform distribution of ozone is prescribed as a function of latitude, height and season. The cloud cover is placed wherever condensation of water vapor is predicted; otherwise, clear sky is assumed. For the computation of terrestrial radiation, the cloud cover is assumed to be a blackbody radiator. For solar radiation, the reflectivity and the absorptivity are prescribed as a function of altitude and cloud thickness. A more detailed description of the cloud prediction scheme will be given in a future publication. One of the important simplifications of this model is the elimination of the diurnal and seasonal variations of insolation. The latitudinal distribution of the annual-mean insolation is prescribed at the top of the model atmosphere for the computation of the solar radiation flux.

The surface temperatures of the continent and the idealized ocean are determined from the boundary condition that no heat is stored at the earth's surface, i.e., that the contributions from the net fluxes of solar and terrestrial radiation and the turbulent fluxes of sensible and latent heat locally sum to zero.

The depth of snow cover and the amount of soil moisture over the continent are computed based on budget equations for snow and soil moisture, respectively [refer to Manabe (1969) for further details]. Differentiation of precipitation between rain or snow is determined by the temperature at a height of ~350 m above the ground. If this temperature is below freezing, it is assumed that snowfall occurs. Otherwise, precipitation occurs in the form of rain. Over the idealized oceanic region, sea ice is predicted where the surface temperature is less than $-2°C$.

For the computation of the heat balance at the earth's surface it is necessary to know the distribution of albedo. The albedos of the soil surface and sea surface are specified as functions of latitude [see Fig. 1 of Manabe (1969) for the latitudinal distributions]. The albedos of snow cover and sea ice are assumed to be much larger than the albedo of bare soil. When the surface temperature is below $-10°C$,[1] the albedos of both snow cover and sea ice are as-

sumed to be 70%. On the other hand, albedos of 45 and 35% are assigned to snow cover and sea ice, respectively, if the surface temperature is above $-10°C$.

3. Numerical time integrations

Numerical time integrations of the model are carried out for three values of the atmospheric CO_2 concentration, viz., 300, 600 and 1200 ppm by volume. Hereafter, these three integrations are identified as standard, $2 \times CO_2$ and $4 \times CO_2$, respectively. By comparing the results from these three experiments, the influences of the increased CO_2 content on the model climate are identified.

Starting from the initial conditions of an isothermal and dry atmosphere, the time integration of the standard experiment is performed over the period of 1200 days. The state of the model atmosphere at the end of the standard integration is chosen as an initial condition for the $2 \times CO_2$ and $4 \times CO_2$ integrations, both of which are carried out over the period of 1200 days. A quasi-equilibrium climate is obtained as the time-mean state of the model atmosphere over the last 500-day period of each integration. As discussed in MW75, the periods of time integration chosen for these experiments are sufficiently long that the response of the model climate to the doubling or quadrupling of CO_2 is much larger than the ambiguity resulting from the failure of the model to completely achieve statistical equilibrium.

Unless specified otherwise, the responses of the model atmosphere to the doubling and the quadrupling of CO_2 are shown as the differences among the time-mean states over the last 500-day period of the three time integrations.

4. Zonal-mean response

The change of the zonal-mean temperature of a model atmosphere in response to the doubling of the atmospheric CO_2 content is extensively discussed in MW75. Despite significant differences between the present model and the MW75 model, the basic characteristics of the zonal-mean temperature response obtained from the present experiments are essentially similar to those obtained in the previous study. Readers should thus refer to MW75 for detailed discussion of the response of the zonal-mean temperature.

However, there are some features of the zonal-mean response which deserve further discussion in this paper. Figs. 2a and 2b show the latitude-height distributions of the zonal-mean temperature response of the model atmosphere to the doubling and quadrupling of CO_2. These figures show that the meridional temperature gradient in the lower troposphere markedly reduces in response to an in-

---

[1] In the study of Manabe and Wetherald (1975), this critical temperature was $-25°C$ because of a code error.
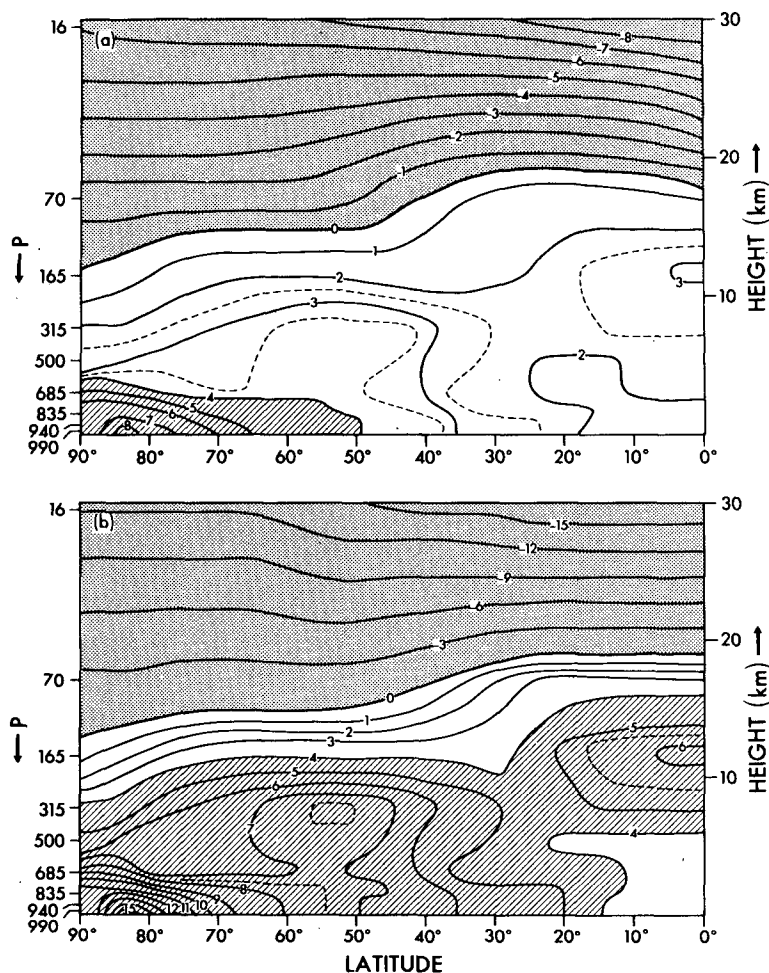
FIG. 2. Latitude-height distribution of the change of the zonal-mean temperature
(K) in response to (a) a doubling of CO_2 content and (b) a quadrupling of CO_2 content.

crease in CO_2. As discussed in MW75, one of the important reasons for this reduction is the enhancement of the warming in high latitudes by the poleward retreat of the highly reflective snow cover and the confinement of the additional heat in the lowest layer of the model troposphere by the stable stratification.

Another important reason for the general reduction of the meridional temperature gradient is the large increase in the poleward transport of latent heat due to the general warming of the model atmosphere. Fig. 3 shows the vertically integrated poleward transport of dry static energy $(C_pT + \phi)$, latent energy (Lr) and moist static energy $(C_pT + \phi + Lr)$ which is the sum of the dry static energy and latent energy. Here T, ϕ and r represent temperature, geopotential height and water vapor mixing ratio, respectively, and C_p and L denote the specific heat of air under constant pressure and the latent heat of evaporation. As shown by this figure, the poleward transport of latent energy at $\sim30°$

latitude increases by as much as 7 and 16% in response to the doubling and quadrupling of CO_2, respectively. The reason for the increased latent heat transport becomes evident when one examines Fig. 4 which presents the latitudinal distributions of the mixing ratio of water vapor at the 940 mb level from all three experiments. This figure indicates that the mixing ratio of water vapor in the lower model troposphere increases markedly with increasing CO_2 content. This is consistent with the highly nonlinear dependence of the saturation vapor pressure of air on temperature. It is therefore reasonable that in a CO_2-rich, warm model atmosphere the poleward transport of latent energy is relatively large, accounts for a major part of the poleward energy transport in middle latitudes, and contributes to the overall reduction of the meridional temperature gradient in the lower troposphere of the model atmosphere.

It is important to recognize, however, that the poleward transport of dry static energy reduces

markedly in response to an increase in CO_2. To a large degree this reduction counterbalances the increase in latent heat transport discussed above. In fact, the poleward transport of moist static energy actually reduces in high latitudes where the meridional temperature gradient reduces markedly mainly due to the reduction of snow-covered area. However, in middle and low latitudes where the influence of snow-cover feedback is less important, the transport of moist static energy increases significantly in response to a doubling of CO_2 as illustrated in Fig. 5. The increase occurs despite the general reduction of the meridional temperature gradient in these latitudes suggesting the increased effectiveness of the model atmosphere in transporting moist static energy poleward.

Recently, using a spectral model of the atmosphere with a limited computational domain, the present authors conducted a series of numerical experiments which are very similar to those described in this paper but with an additional case where the CO_2 concentration was increased eight times the normal amount ($8 \times CO_2$). It was found that, owing to a relatively high surface air temperature, snow cover is absent from the $8 \times CO_2$ experiment and almost absent from the $4 \times CO_2$ experiment. The comparison between these two experiments indicates that, in the absence of the snow-albedo feedback mechanism, the poleward transport of moist static energy increases at all latitudes and the equator-to-pole difference of surface air temperature reduces by $2-3°C$ in response to this particular range of CO_2 increase (refer to Fig. 5). Qualitatively, a similar increase of the moist static energy transport was noted by Held (1978) in his results from a set of numerical experiments with a simple general circulation model.

These results convince the authors that the effectiveness of the atmospheric circulation as a whole for transporting moist static energy increases with increasing atmospheric temperature and results in the reduction of the meridional temperature gradient in the lower model atmosphere. In other words, the meridional temperature gradient in the lower troposphere is reduced irrespective of the existence of the snow-albedo feedback mechanism. The increase in the poleward moisture transport which is discussed above is responsible for this change.

It is probable that the large reduction in the meridional temperature gradient in the middle and lower model troposphere, which is discussed above, alters the distribution of the eddy kinetic energy. Fig. 6 shows the latitude-height distribution of the eddy kinetic energy change caused by the quadrupling of CO_2. As discussed in MW75, eddy kinetic energy reduces in the middle and lower model troposphere probably because of the reduction of the meridional temperature gradient. On the other hand, it increases
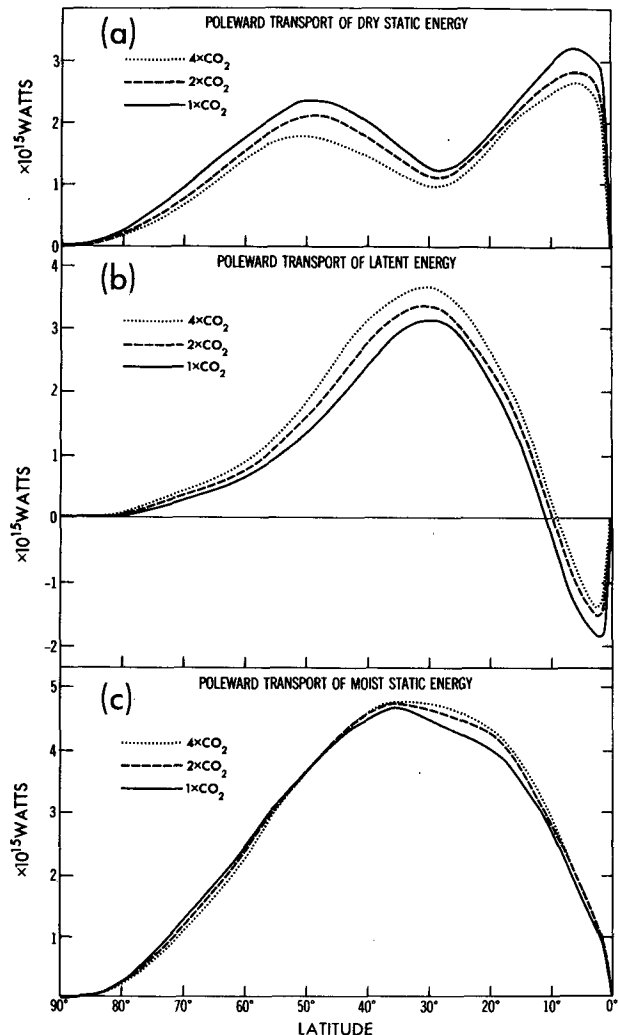

FIG. 3. Vertically integrated poleward transport of (a) dry static energy ($C_pT + \phi$), (b) latent energy (Lr) and (c) moist static energy ($C_pT + \phi + Lr$). Negative values are equatorward transport.

in the upper model troposphere where the static stability decreases as Fig. 2 indicates. Further study is required for the definitive determination of the basic cause for the change in the distribution of eddy kinetic energy described above.

An increase in CO_2 content affects not only the distribution of eddy kinetic energy, but also the variability of temperature in the model atmosphere. Fig. 7b shows the latitude-height distribution of the change in the variance of the temperature fluctuation $(\overline{T'^2})^\lambda$ in response to the quadrupling of CO_2 content. Here, ( )$'$ denotes the deviation from the time mean, and ($^-$)^t and ($^-$)$^\lambda$ indicate the time and zonal means, respectively. As a reference, the latitude-height distribution of temperature variance in the standard model atmosphere is presented in Fig. 7a.
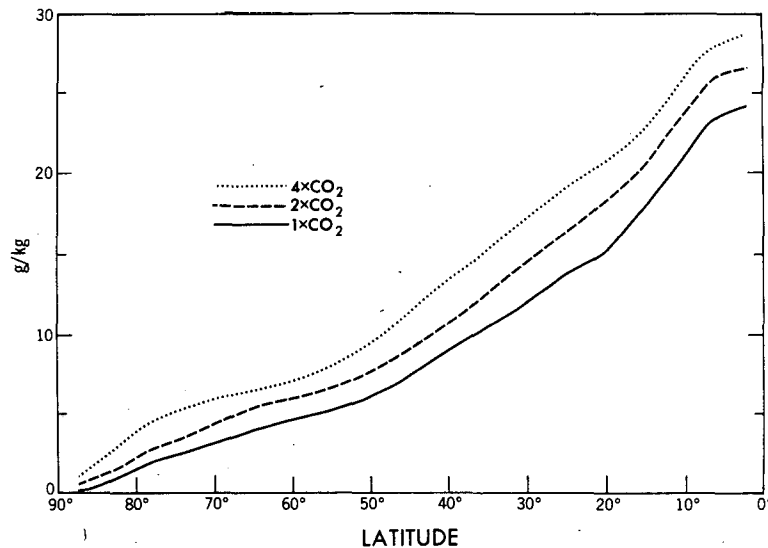
FIG. 4. Latitudinal distribution of the zonal-mean water vapor mixing ratio at the
940 mb level from the three experiments.

Fig. 7b indicates that the variance of temperature increases somewhat in the upper model atmosphere but decreases markedly in the lower model troposphere in response to the quadrupling of CO_2 content in air. This decrease is particularly large in middle and high latitudes. It therefore appears that the general reduction of the meridional temperature gradient in response to the CO_2 increase is responsible for the reduction of both the eddy kinetic energy and the variance of temperature in the lower model troposphere.

The increase in the poleward transport of latent energy discussed above has a very important hydrologic implication. In MW75 it was emphasized that the area-mean rate of precipitation increases markedly in response to an increase of CO_2. A similar increase is evident in the upper half of Fig. 8a, which shows the latitudinal distributions of the zonal-mean precipitation rate from the standard, 2 × CO_2 and 4 × CO_2 experiments. Although the increase in evaporation rate tends to be uniform at most latitudes, as Fig. 8b indicates, the increase in precipitation rate is not uniform at all latitudes. It is particularly large poleward of 45° latitude, and far exceeds the increase of the evaporation rate. Also evident is the poleward shift of the latitude of the maximum precipitation rate in middle latitudes as the CO_2 concentration is increased. The large in-
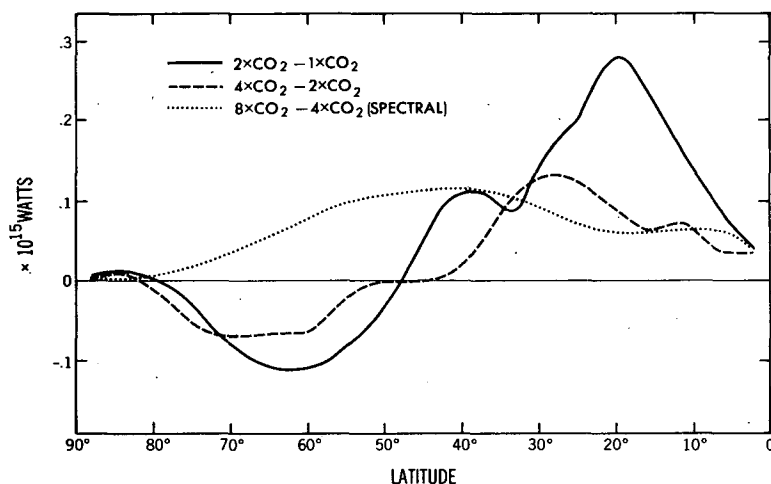

FIG. 5. Latitudinal distribution of the change of the poleward transport of moist
static energy between the successive experiments of this study. The last category
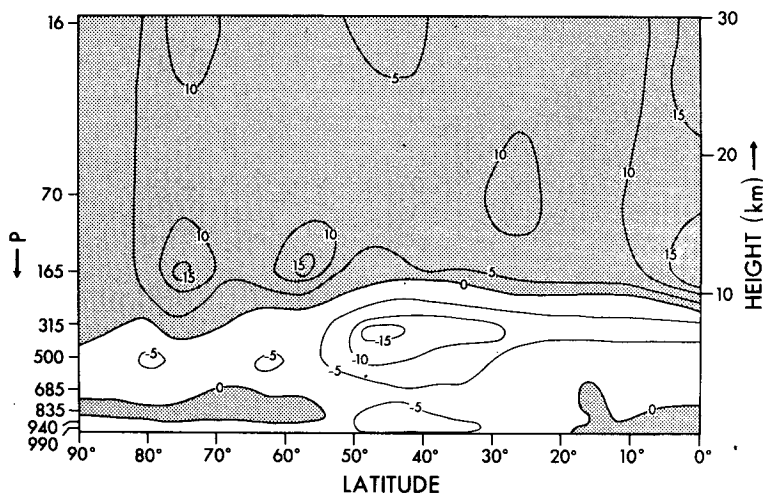(4 × CO_2 → 8 × CO_2) was obtained from a spectral version of the current model.

FIG. 6. Latitude-height distribution of the zonal-mean change of eddy kinetic energy (J kg^{-1}) due to a quadrupling of CO_2 content.
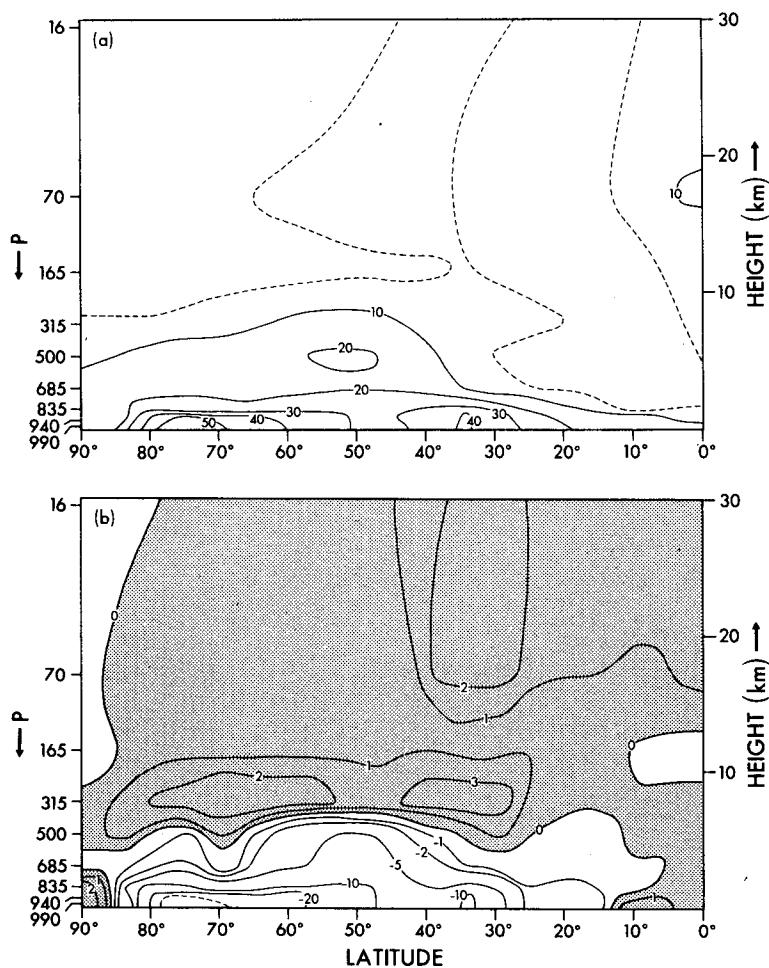

FIG. 7. Latitude-height distribution of (a) the zonal-mean variance of temperature from the standard experiment and (b) the change of the zonal-mean variance of temperature due to a quadrupling of CO_2 content. Units are K^2.
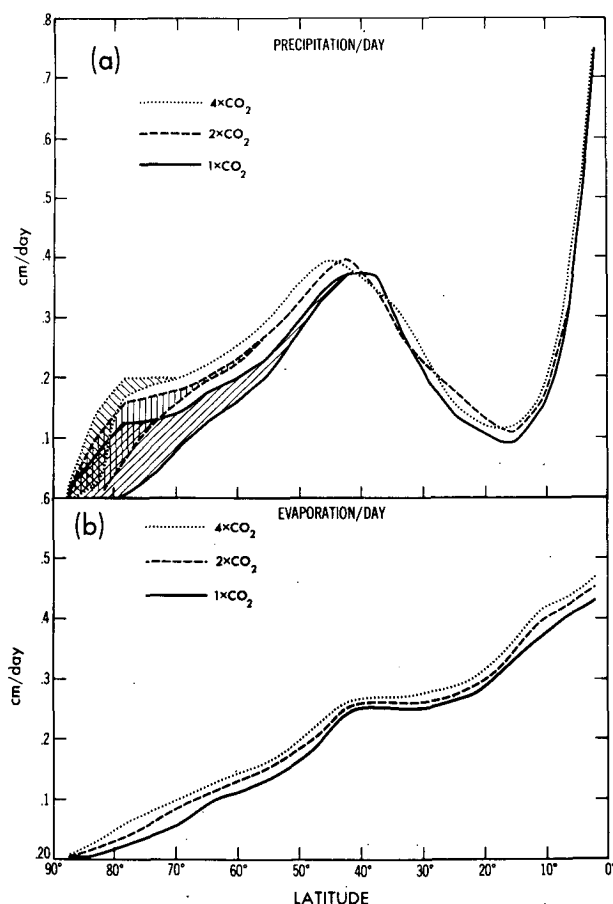
FIG. 8. Zonal-mean rates from all three experiments of (a) total precipitation and (b) evaporation. The portion of the precipitation rate, which is attributable to snowfall, is indicated by various types of cross hatching.

crease in the precipitation rate in high latitudes obviously results from the large increase in the poleward transport of water vapor into higher latitudes, where the moisture content of air increases markedly (see Fig. 4). As discussed later, the changes in the rates of precipitation and evaporation have a profound effect on the hydrology over the model continent, namely they yield large excesses of moisture in high latitudes and some deficit in a certain region of the middle latitudes.

5. Area-mean response

Table 1 contains the changes of the area-mean surface air temperature of the model in response to the doubling and quadrupling of CO_2 content. As shown by this table, the sensitivity of the present model is approximately similar to the sensitivity of the previous model (MW75) despite the incorporation of the cloud-radiation feedback mechanism into the present model. The influence of the cloud-radiation feedback mechanism is discussed in Section 8.

Table 1 also reveals that the change in surface air temperature of the model is almost linearly proportional to the change in the logarithm of the CO_2 amount. A similar relationship is evident in Figs. 2a and 2b which show the response of the zonal-mean temperature of the model atmosphere to the doubling and quadrupling of the CO_2 content. It holds because the emissivity of carbon dioxide is almost linearly proportional to the logarithm of carbon dioxide amount in the range under consideration. A similar relationship emerged in the result of Manabe and Wetherald (1967) from their one-dimensional model of radiative-convective equilibrium. For reference, Table 1 also tabulates the responses of the one-dimensional (1-D) radiative-convective equilibrium model which incorporates the scheme of radiative computation used for the present three-dimensional (3-D) model. A quasi-linear relationship is also evident in this result. One can evaluate the validity of this relationship further by referring to the studies of Rasool and Schneider (1971) and Augustsson and Ramanathan (1977) with simple global-average models.

It is of interest that the surface-air temperature is more sensitive to the increase of CO_2 content in the 3-D model than in the 1-D model. As discussed in MW75, the larger sensitivity of the 3-D model is caused, in part, by the inclusion of the so-called snow-albedo/surface temperature feedback mechanism in the model.

The area-mean changes of precipitation rate in response to the doubling and quadrupling of CO_2 in the model atmosphere are given in Table 2. This table shows that the area-mean precipitation rate increases by 12% when the CO_2 content is quadrupled. As discussed in Section 7, the temperature change in the model atmosphere due to the quadrupling of CO_2 is very similar in magnitude and distribution to the change caused by a 4% increase in the solar constant. However, as noted above, the intensity of the hydrologic cycle increases by a percentage which is much larger than 4%. Wetherald and Manabe (1975) found a similarly excessive increase in the intensity of the hydrologic cycle in response to an increase of the solar constant and concluded that it results from 1) the decrease of Bowen's ratio with increasing surface temperature and 2) the increase in the downward terrestrial radiation due to

TABLE 1. Area-mean surface air temperature difference (K) obtained from a doubling and quadrupling of CO_2 content. Results from the one-dimensional (1-D) radiative, convective model are added for comparison.

	1-D	3-D
$2 \times CO_2$	2.0	3.0
$4 \times CO_2$	4.1	5.9

the nonlinear increase of the water vapor content of air with respect to increasing temperature. In this study similar changes of the model atmosphere occur in response to an increase of CO_2 content of the atmosphere.

6. Geographical response

It is found that the doubling and quadrupling of CO_2 has a significant influence not only on the zonal- and area-mean climates, but also on the geographical distribution of climate, particularly of the hydrologic variables. Therefore, this section is mainly devoted to the geographical distributions of the hydrologic response to the increase of CO_2 content.

Before beginning a detailed discussion of the geographical response, it is desirable to describe briefly the surface climatology from the standard experiment. Fig. 9a shows the geographical distribution of the precipitation rate from the standard experiment. In this distribution, one can identify the tropical rainbelt, the subtropical dry belt and the mid-latitude rainbelt. In addition, one notes the region of relatively large precipitation rate along the east coast of the subtropical portions of the model continent. As Manabe (1969) pointed out, the northward advection of moist air and the northward migration of cyclones along the periphery of the oceanic anti-cyclone in the model subtropics account for the relatively large precipitation rate in the coastal region. Fig. 9b shows the geographical distribution of the evaporation rate and indicates that the evaporation rate over the continent is much less than that over the ocean in the model subtropics. This land-sea contrast in evaporation rate produces the land-sea contrast in surface temperature and, accordingly, sea level pressure. In Fig. 10, which shows the geographical distribution of the sea level pressure of the model atmosphere, one can identify an' anticyclone in the subtropical ocean where the surface temperature is relatively low because of the heat loss due to a high evaporation rate. Along the western periphery of this oceanic anticyclone, moisture is transported poleward, as Fig. 11 indicates, and contributes to the enhancement of precipitation along
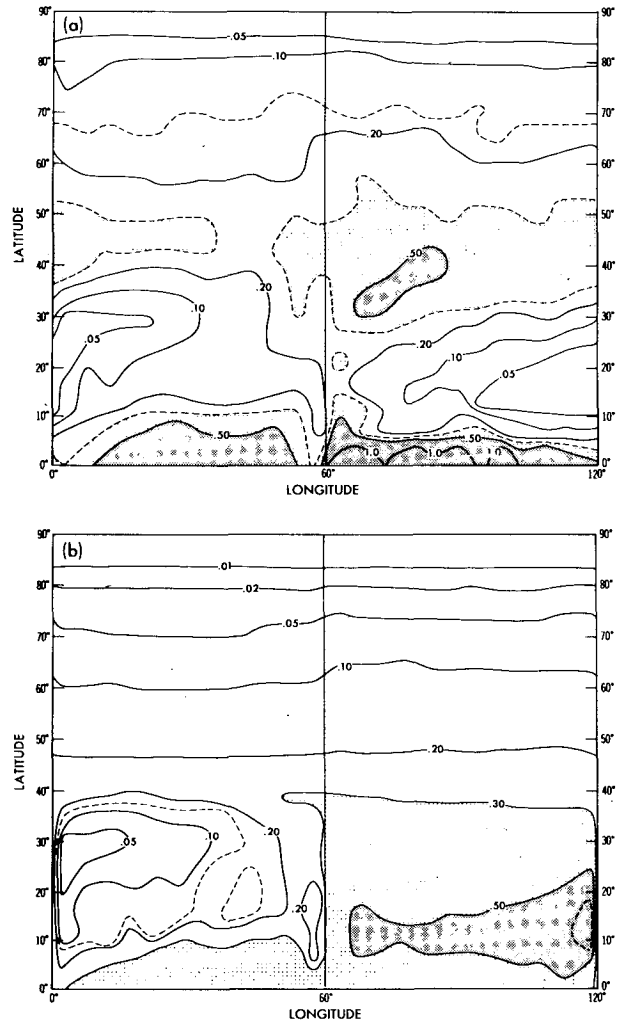

Fig. 9. Horizontal distributions of (a) total precipitation rate and (b) evaporation rate which are obtained from the standard experiment. Units are cm day^{-1}.

the east coast of the model continent. (In Fig. 11, the moisture transport vector m is defined as

$$\mathbf{m} = \frac{1}{g} \int_0^{P_*} \bar{v}^t r dp,$$

where g is the acceleration of gravity, r the mixing ratio of water vapor, $\bar{v}^t$ the time mean wind vector, p the pressure and P_* the surface pressure.) The monsoonal precipitation discussed above influences the geographical distribution of soil moisture which is shown in Fig. 12. According to this figure, soil moisture in the subtropical portion of the continent is relatively large along the east coast and becomes very small near the west coast in response to the longitudinal variation of the precipitation rate which is illustrated in Fig. 9a.

In the high-latitude portions of the model continent where the precipitation rate substantially ex-

TABLE 2. Area-mean precipitation rate $\bar{P}^A$ (cm day^{-1}) and fractional increase of area-mean precipitation rate due to a doubling and quadrupling of CO_2. $\bar{P}^A_{1\times CO_2}$ is the area mean precipitation rate from the standard (1 × CO_2) experiment.

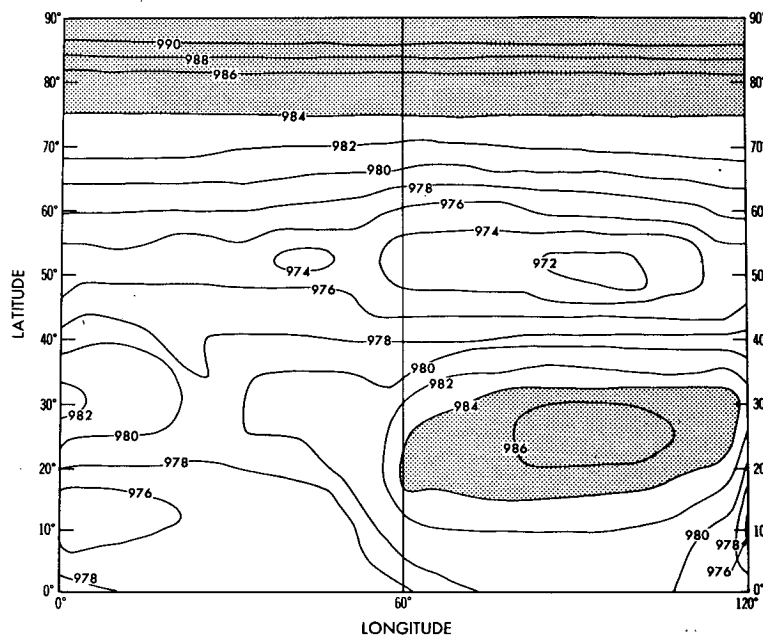|	$\bar{P}^A$	$\dfrac{\bar{P}^A - \bar{P}^A_{1\times CO_2}}{\bar{P}^A_{1\times CO_2}}$
1 × CO_2	0.258	0
2 × CO_2	0.276	0.07
4 × CO_2	0.288	0.12

FIG. 10. Horizontal distribution of the surface pressure (mb) from the
standard experiment.

ceeds the evaporation rate, the soil is nearly satu-
rated with water. In low latitudes, the soil moisture
increases from the subtropics to the tropics of the
model where the tropical rainbelt is located. How-
ever, because the precipitation is highly sporadic
in the model tropics, the time-mean value of the soil
moisture there is significantly below the saturation

value of 15 cm even though the time-mean rate of
precipitation far exceeds that of evaporation. One
can appreciate that the larger the variability of the
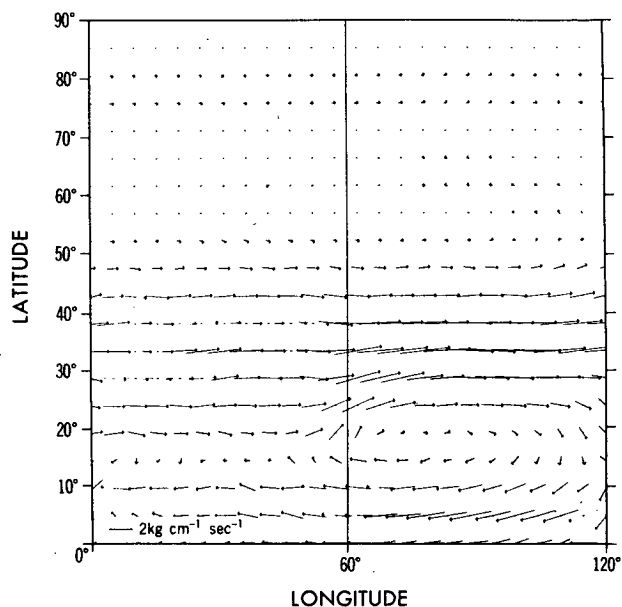precipitation rate, the greater is the fraction of rain-

FIG. 11. Horizontal distribution of the moisture transport
vector m for the standard experiment. For the scaling of a vec-
tor, see the line segment indicating 2 kg cm⁻¹ s⁻¹ in the lower
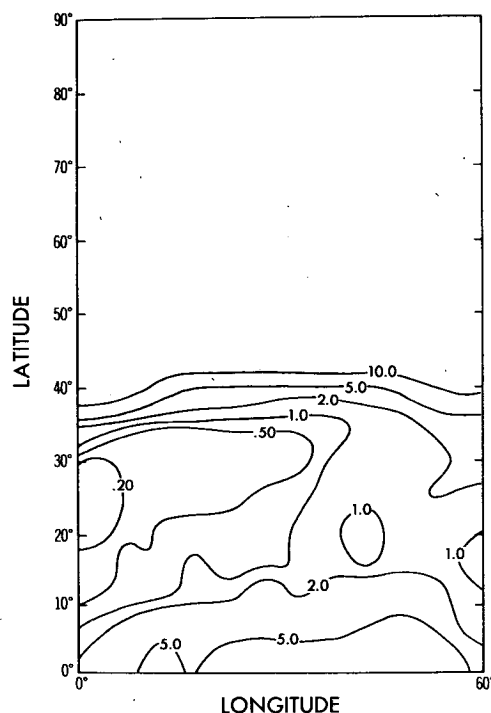left corner of the figure.

FIG. 12. Horizontal distribution of the soil moisture (cm) over
the continent for the standard experiment. (For this study, it is
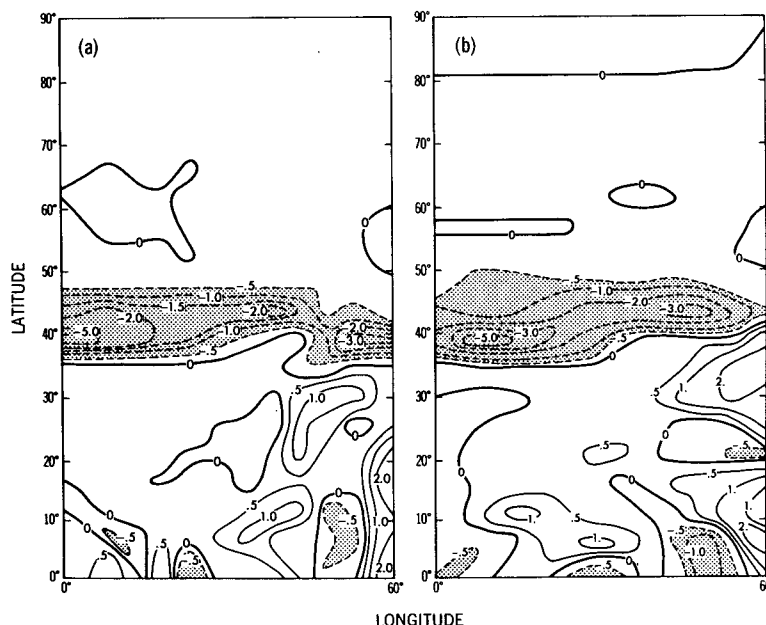assumed that the field capacity of soil is 15 cm everywhere.)

FIG. 13. Horizontal distribution of the change of soil moisture (cm) over the continent in response to (a) a doubling of CO_2 content, (b) a quadrupling of CO_2 content.

water diverted to runoff and thus the less the soil moisture.

The geographical distributions of climate and hydrology, which are briefly described above, are essentially similar to those discussed by Manabe (1969). Refer to his paper for further discussion of this subject.

The distribution of soil moisture changes significantly when the CO_2 content of air is increased. Figs. 13a and 13b illustrate the geographical distributions of the changes in soil moisture over the model continent in response to the doubling and quadrupling of CO_2 content, respectively. One of the notable features common to both distributions is the reduction of soil moisture in the zonal belt located between 37 and 47° latitude. This drying is also indicated in Fig. 14, which shows the zonal-mean values of precipitation rate (P), that of evaporation rate (E) and $(P - E)$ over the model continent as a function of latitude. [Note that $(P - E)$ is approximately equal to the runoff rate. In the absence of a systematic change of soil moisture with time, the difference between the time mean rates of precipitation and evaporation is essentially equal to that of runoff.] As shown by this figure, the precipitation rate decreases slightly in the zonal belt mentioned above due to the poleward shift of the rainbelt in middle latitudes. Therefore, as Fig. 14c indicates, $(P - E)$ and, accordingly, runoff rate over the model continent decrease significantly between 40 and 50° latitude causing the substantial reduction of the soil moisture there.

In Section 4, it was shown that the eddy kinetic energy in the middle and lower troposphere decreases in response to a CO_2 increase, probably because of a reduction in the meridional temperature gradient. This decrease is particularly large around 40–45° latitude where the meridional temperature gradient is reduced significantly throughout the entire model troposphere as Fig. 2 indicates. In Fig. 15, which shows the geographical distribution of the change in eddy kinetic energy at the 500 mb level, one can identify the zonal belt of eddy kinetic energy reduction at around 45° latitude over the model continent. It is probable that this reduction is partly responsible for the decrease (or lack of significant increase) in precipitation rate and for the drying of the soil in this zonal belt.

According to Fig. 14c, $(P - E)$ increases markedly poleward of 50° latitude in response to the increase of the CO_2 content. The significant increase in the poleward moisture transport, which was discussed in Section 4, is responsible for this change. In short, a marked increase in the runoff rate occurs in higher latitudes of the model because of an increase in CO_2 content of air.

Another feature of interest, which is common to both Figs. 13a and 13b, is the general increase in soil moisture along the east coast of the continent equatorward of 35° latitude. This change results from the increase in the aforementioned monsoonal precipitation which is caused by the intensification of the northward moisture transport along the periphery of the oceanic anticyclone in the model sub-
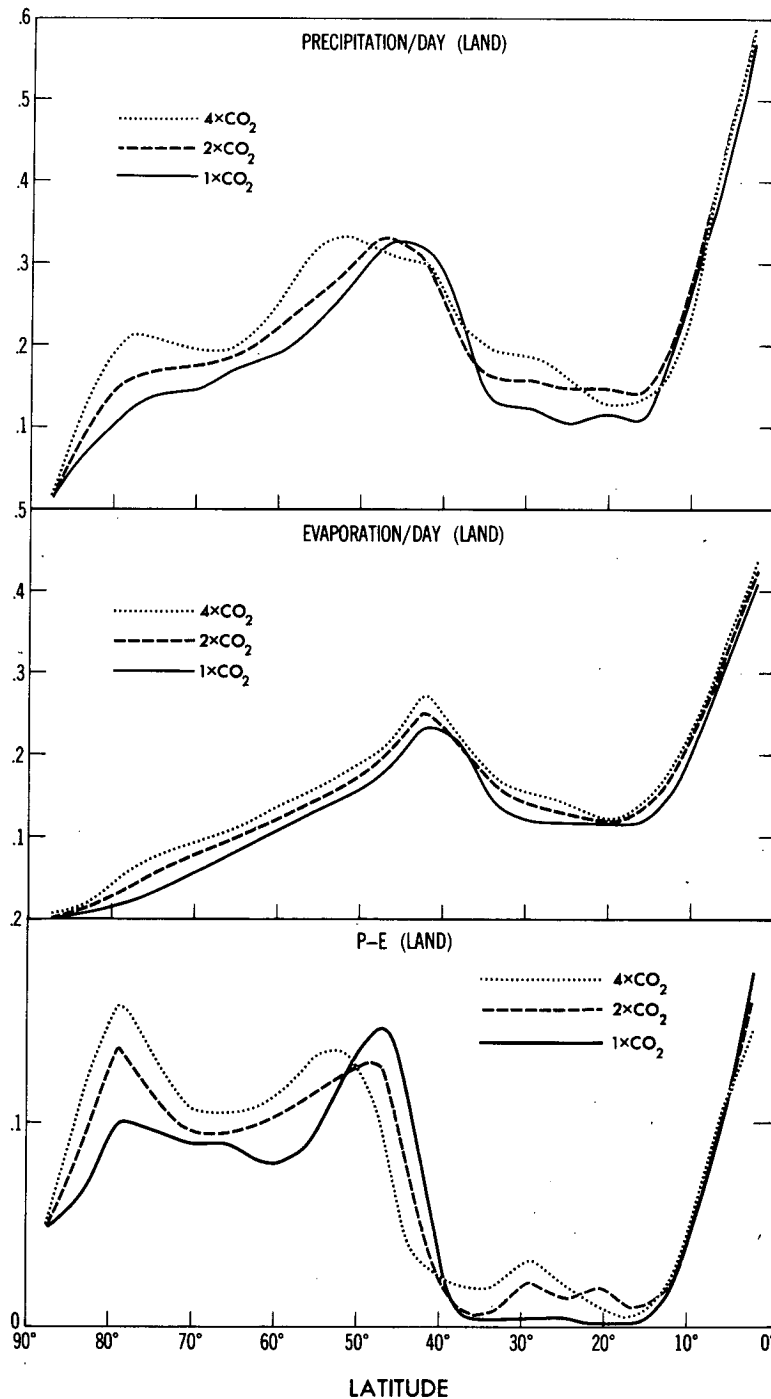
FIG. 14. Zonal-mean values of (a) precipitation rate, (b) evaporation rate and (c) precipitation rate minus evaporation rate, i.e., $(P - E)$, over the continent from all three experiments. Units are cm day^{-1}.

tropics. This intensification is mainly caused by an increase in the moisture content of the air, and is evident in Fig. 16 which shows the change in the moisture transport vector in response to the quadrupling of CO_2 content in the model atmosphere. The change in the monsoonal precipitation manifests

itself in Fig. 17, which shows the geographical distribution of the change in $(P - E)$ in response to the doubling of CO_2. According to this figure, $(P - E)$ increases along the east coast of the model continent in both the subtropics and the tropics. In addition, this figure reveals that $(P - E)$ de-
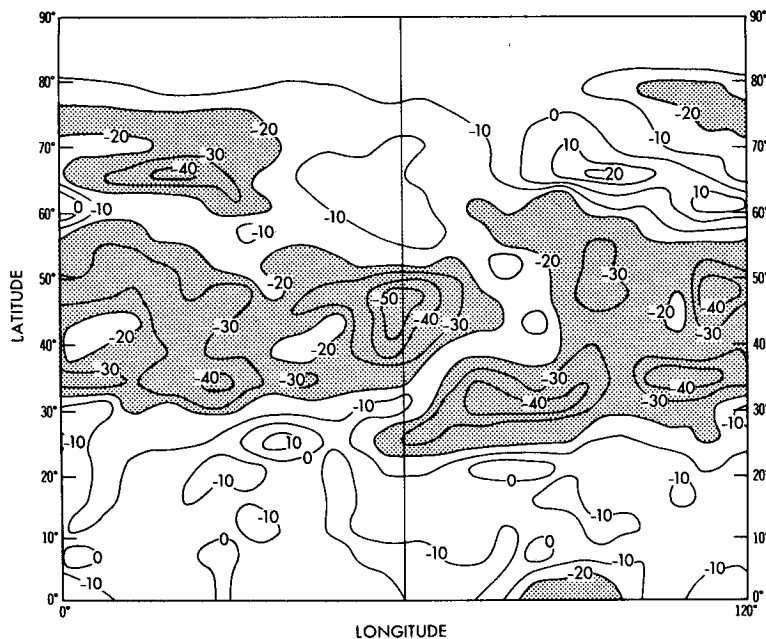
Fig. 15. Horizontal distribution of the change of eddy kinetic energy ($J\ kg^{-1}$) at the 500 mb level of the model atmosphere in response to a quadrupling of the CO_2 content.

creases over the model continent around 45° latitude as discussed above. It should be noted here that, over the model continents, the distribution of ($P - E$) shown in Fig. 17 is essentially similar to the distribution of the runoff rate as pointed out earlier.

The change in the wetness of the soil surface significantly affects the change of surface air temperature shown in Fig. 18a. According to this figure, warming over the model continent has a local maximum around 40° latitude where the soil moisture decreases. On the other hand, warming is relatively small along the east coast of the model continent where the soil moisture increases. One can appreciate these results by recognizing the influence of the soil moisture on the rate of evaporation. For example, the reduction of soil moisture results in the suppression of heat loss by evaporation from the continental surface and contributes to the warming of the surface temperature. In high latitudes, warming is at a maximum around 83° latitude where the surface albedo reduces the most as indicated in Fig. 18b owing to the poleward retreat of the snow cover and sea ice.

The results described above suggest that the climatic consequences of increasing CO_2 are far from uniform and are highly variable geographically.

7. Increased solar constant

Recently, the present authors conducted a series of numerical time integrations of the model assuming various values of the solar constant. It was found

that the comparison between this set of solar constant experiments and the present CO_2 experiments revealed the relative importance of the mechanisms for the reduction of the meridional temperature gradient which are discussed in Section 4. There-
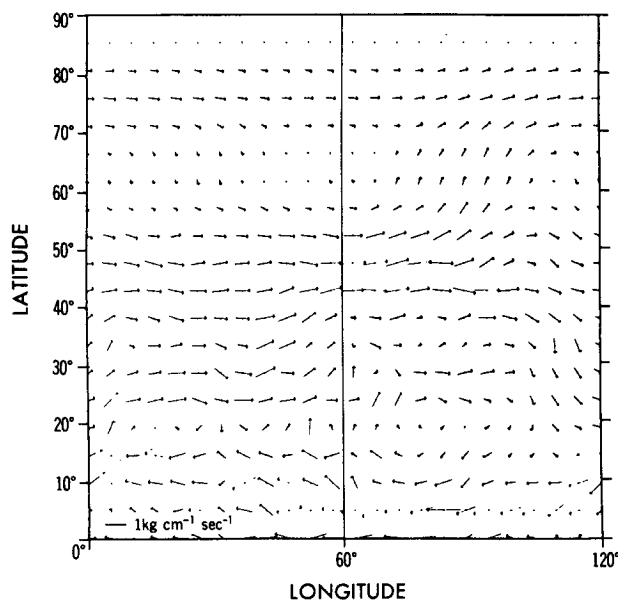

Fig. 16. Horizontal distribution of the change of the moisture transport vector m in response to a quadrupling of the CO_2 content. For the scaling of a vector see the line segment indicating 1 kg cm^{-1} s^{-1} in the lower left corner of the figure.
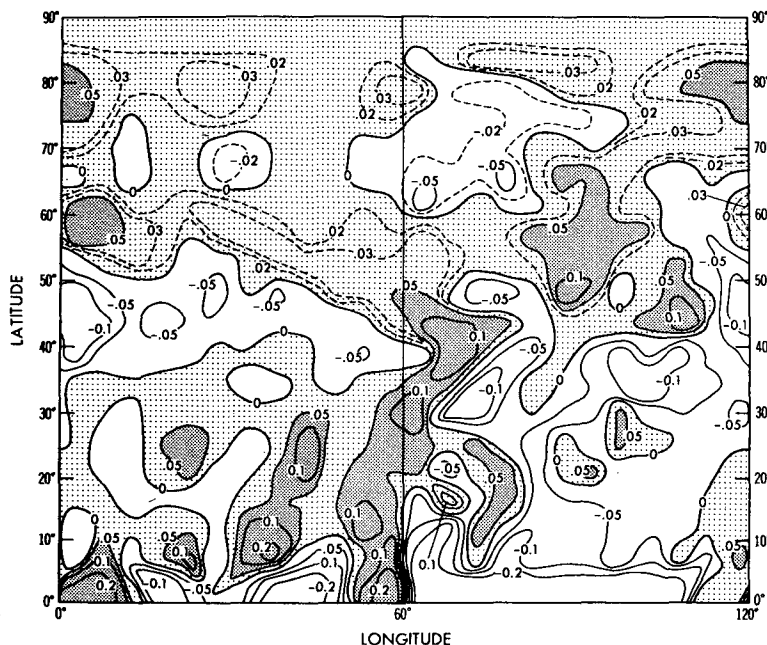
FIG. 17. Horizontal distribution of the change of precipitation rate minus evaporation rate, i.e., $(P - E)$, in response to a doubling of CO_2 content. Units are cm day^{-1}.

fore, it was decided to discuss the results from this comparison.

The model structure and the time integration procedure, which were adopted for the solar constant experiments, were identical to those of the CO_2 experiments which are described in Sections 2 and 3. The results, which are shown here for the comparison, represent the time averages over the last 500 days of each integration. Further details of the experiments are contained in a forthcoming paper which discusses the influences of cloud cover on the sensitivity of the model climate.

In Fig. 19, the changes in the zonal-mean surface air temperature in response to the doubling and the quadrupling of CO_2 content are compared with the corresponding changes due to a 2% and a 4% increase in the solar constant. This figure clearly indicates that the latitudinal distribution of the change in the zonal-mean surface air temperature resulting from the doubling (or quadrupling) of CO_2 closely resembles the change due to a 2% (or 4%) increase in the solar constant. This resemblance is particularly surprising because the radiative influence of a CO_2 increase is quite different from that of an increased solar constant as discussed below.

Fig. 20a shows the latitudinal distributions of the changes in the net downward radiative flux at the 200 mb level of the standard model atmosphere when the CO_2 content of air is quadrupled or the solar constant is increased by 4% but all other relevant parameters of the model (i.e., air temperature, mix-

ing ratio of water vapor and the surface albedo of the earth's surface) are held fixed. Since the 200 mb level approximately corresponds to the tropopause level, the new downward flux indicates the net acquisition of heat by the troposphere-earth system. According to this figure, the latitudinal distribution of the radiative heat gain by the troposphere-earth system resulting from the quadrupling of CO_2 content is significantly different from the distribution of heat gain due to a 4% increase of the solar constant. However, both distributions yield approximately the same increase in net radiative heating when they are averaged over the entire computational domain.

In Section 4 it was noted that the general warming of the entire model troposphere reduces the area of highly reflective snow cover in high latitudes, enhances the poleward transport of latent energy and thus reduces markedly the meridional temperature gradient. In other words, the overall warming of the model atmosphere affects not ony the area-mean temperature but also the latitudinal gradient of temperature of the model atmosphere. It is found that this effect is so overwhelming that the difference between the latitudinal distributions of the two thermal forcings described above has a relatively minor effect in altering the meridional temperature gradient of the model atmosphere. This is evident in Fig. 20b which shows the contributions of the relevant factors to the change in the heat balance of the earth-atmosphere system of the model which
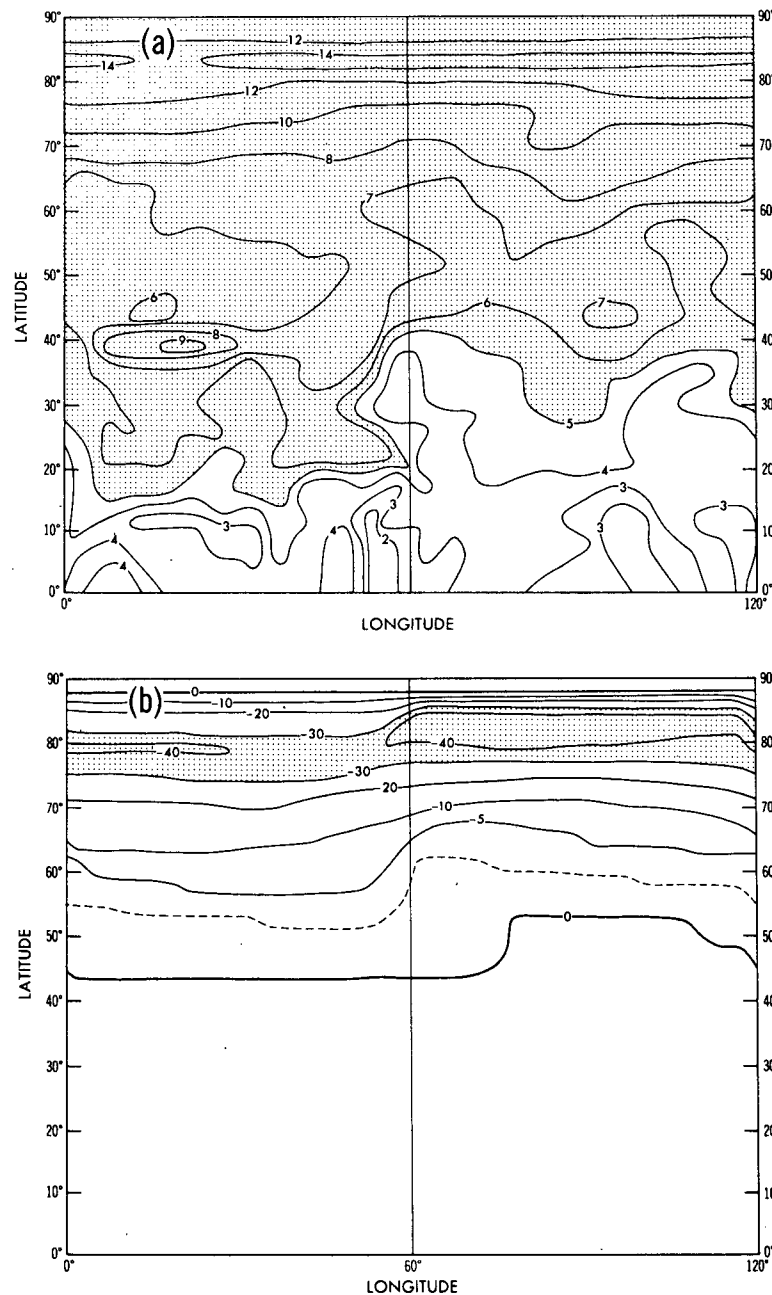
FIG. 18. Horizontal distribution of the change of surface-air temperature (K) in response to a quadrupling of CO_2 content (a) and horizontal distribution of the change of surface albedo (%) in response to a quadrupling of CO_2 content (b).

results from the quadrupling of the CO_2 content. In this figure, the dashed line shows the latitudinal distribution of the change in the net downward solar radiation at 200 mb which is mainly attributable to the reduction of surface albedo. The solid line shows the latitudinal distribution of the change in the net release of latent energy (i.e., the difference between the heat released by condensation and the heat consumed by evaporation) in the earth-tropo-

sphere system of the model. This change is the consequence of the general increase in the poleward transport of latent energy. For the sake of comparison, the difference between the two radiative forcings shown in Fig. 20a is added to Fig. 20b. This figure clearly indicates that the consequences of the general warming (i.e., snow cover reduction and the increase in latent heat transport) contribute significantly to the reduction of the meridional tempera-
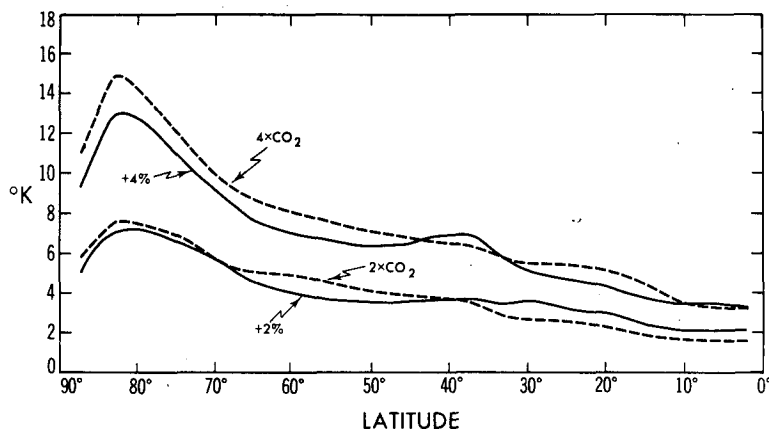
FIG. 19. Latitudinal distribution of the zonal-mean change of surface air temperature in response to a 2% (and a 4%) increase of the solar constant, and a doubling (and quadrupling) of the CO_2 content.

ture gradient. The first effect is particularly important at high latitudes but the second effect exerts its influence at all latitudes. The magnitudes of these contributions are much larger than the difference
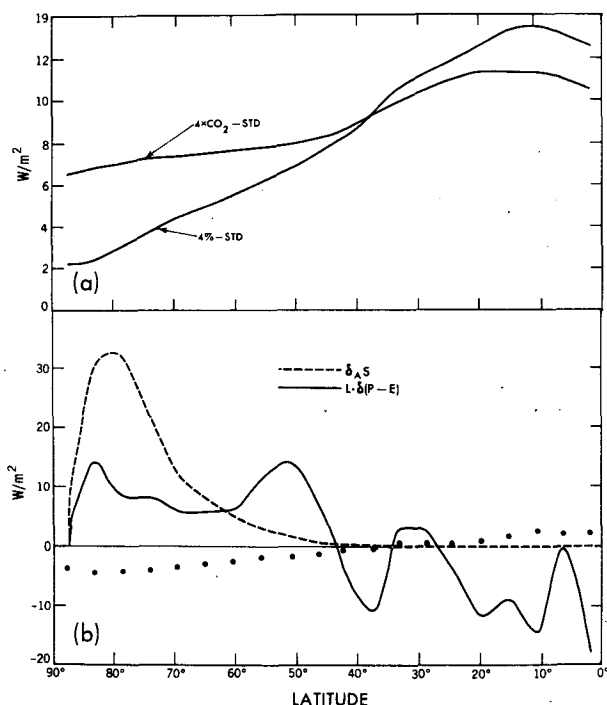

FIG. 20. (a) Latitudinal distribution of the change in net downward radiation flux at the 200 mb level of the standard model atmosphere. A change is computed by either quadrupling the CO_2 content or increasing the solar constant by 4% and keeping all other relevant factors unchanged.

(b) Dashed line indicates the latitudinal distribution of the change in zonal-mean net downward solar radiative flux at the 200 mb level of the standard model atmosphere which is attributable to the reduction of surface albedo resulting from the quadrupling of the CO_2 content. Solid line shows the change in the net release of latent energy $L(P - E)$ in the earth-atmosphere system of the model due to the quadrupling of the CO_2 content. Dots indicate the difference between the two thermal forcings shown in Fig. 20a.

between the latitudinal distributions of the two radiative forcings confirming the statement made earlier. Since the area-mean warming due to the quadrupling of CO_2 is very similar in magnitude to the warming resulting from the 4% increase of the solar constant, it is reasonable that the reductions of the meridional temperature gradient due to these two forcings are approximately similar to one another.

The similarity between the results from the CO_2 and solar constant sensitivity studies is also evident in the geographical distribution of the changes in hydrologic variables. Fig. 21 shows the horizontal
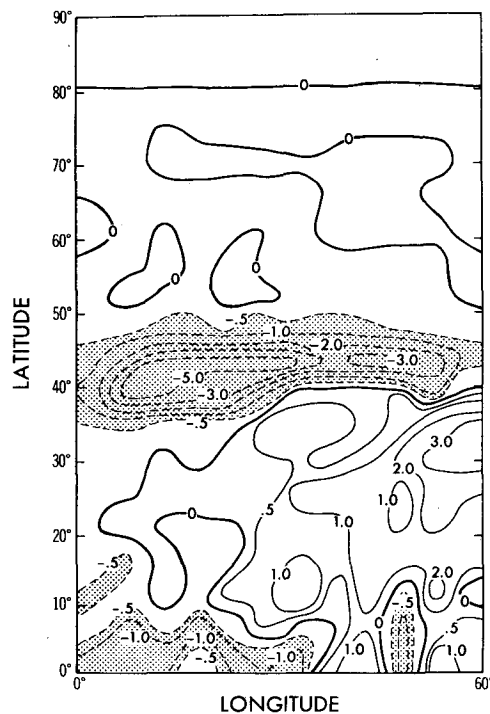

FIG. 21. Horizontal distribution of the change of soil moisture (cm) over the continent in response to a 4% increase of the solar constant.

distribution of the change in soil moisture over the model continent in response to the 4% increase of the solar constant. The general features of the distribution are very similar to the distribution of soil moisture change in response to the quadrupling of CO_2 content which was shown in Fig. 13b and discussed in Section 6. For example, Figs. 21 and 13b both indicate a zonal belt of enhanced aridity around 42° latitude and increased wetness along the east coast of the subtropical and tropical continent.[2] This similarity reinforces the statistical significance of the changes of surface aridity which are discussed in Section 6.

8. Cloud response

As discussed in the Introduction, one of the significant differences between this study and that of MW75 is the incorporation of the cloud/radiation feedback mechanism into the present model. Therefore, it is decided to discuss briefly here the influence of the cloud cover change on the response of the model climate to the increase in CO_2 content.

Fig. 22a is the latitude-height distribution of the zonal-mean cloud amount obtained from the standard experiment. This figure indicates that the cloud amount in the model atmosphere has a local maximum in the tropics and midlatitudes and a minimum in the subtropics where the downward motion branch of the Hadley cell is located. It also indicates that the layer of relatively large cloud amount which is located at ~12 km in the tropics and at ~6 km in high latitudes may be identified as a layer of cirrus cloud. One can also identify a layer of relatively large cloud amount which is located just above the earth's surface in high latitudes of the model as low stratus cloud. The characteristics of the zonal-mean cloud distribution in the standard model atmosphere, which are described above, are evident in the actual cloud distribution as estimated by Telegadas and London (1954) and London (1957).

As one might expect from the discussions in the preceding section, the distribution of cloud cover change, which results from an increase in the CO_2 content of air, is very similar to the corresponding distribution of cloud cover change caused by an increase in the solar constant. The latter distribution will be extensively discussed in the future publication which deals with the influence of cloud cover on the sensitivity of the model climate. Nevertheless, a brief discussion of the former is presented here for the present readers.
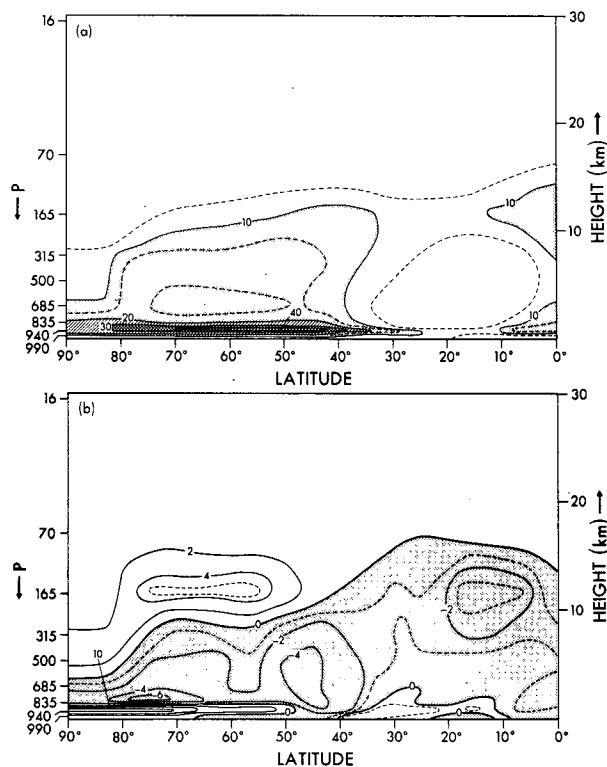

Fig. 22. Latitude-height distribution of (a) the zonal-mean cloud amount from the standard experiment and (b) the change of the zonal-mean cloud amount in response to a quadrupling of the CO_2 content. Units are percent.

The change of the zonal-mean cloud amount, which occurred in response to the quadrupling of CO_2, is shown as a function of latitude and height in Fig. 22b. This figure indicates that, in the upper and middle troposphere, cloudiness decreases at most latitudes. [Qualitatively, a similar reduction of cloudiness was noted and discussed by Roads (1978) and Schneider et al. (1978) when they examined the cloudiness change in their model atmosphere which occurred in response to an increase in sea-surface temperature.] On the other hand, low cloudiness increases in the lower troposphere of high latitudes and the subtropics where the relatively stable stratification reduces the penetration of moisture into the mid-troposphere and relative humidity increases due to the enhanced evaporation from the earth's surface. In addition, cloudiness increases in the lower stratosphere of the model. It is found that the large reduction in static stability around the tropopause level, a result of the large difference in warming between the troposphere and the stratosphere, enhances the convergence of the upward moisture transport into the lower stratosphere and raises the relative humidity and cloudiness there. In summary, cloudiness decreases in the upper and middle troposphere of the model at most latitudes but increases near the earth's surface and lower model stratosphere in high latitudes in response to

---

[2] The present authors performed a series of numerical experiments comparable to those described in this section with a version of the model in which the cloud distribution was held fixed. It was found that the inclusion of cloud feedback did not significantly alter the basic characteristics of the changes in the soil moisture distribution which are identified here. For the discussion of the effect of the cloud feedback mechanism on the sensitivity of zonal-mean climate, see Section 8.

TABLE 3. Partial change in S, F and R (W m^{-2}) of the standard model atmosphere attributable to the separate change in various relevant factors, i.e., CO_2, T, r, A and C. Σ denotes the sum of all these partial changes. δY is the change in a radiative flux Y (i.e., S, F or R) due to the simultaneous changes in all relevant variables resulting from the quadrupling of CO_2.

| $y\backslash x$ | $\overline{\delta_x Y^A}$ | | | | | Σ | δy |
	CO_2	T	r	A	C		
S	0.35	—	1.12	2.10	2.26	5.83	5.72
$-F$	4.26	−16.74	6.68	—	−2.06	−7.86	5.72
R	4.61	−16.74	7.80	2.10	0.20	−2.03	0

an increased CO_2 content. Because of these changes, both total cloudiness and the effective cloud-top height reduce equatorward of 50° latitude. However, total cloudiness as averaged over the entire computational domain changes little ($<1\%$) because of the increase in total cloudiness in the region poleward of 50° latitude. (Here, total cloudiness means the fraction of horizontal area covered by clouds.)

For the evaluation of the relative importance of the cloud changes presented above, an analysis of the radiative fluxes has been performed. The method of analysis involves the computation of the contribution of the change in each relevant factor on the changes of solar and terrestrial radiative fluxes at the top of the model atmosphere.

The change in the net downward radiation at the top of the model atmosphere in response to the quadrupling of CO_2 content is given by

$$\delta R = \delta S - \delta F, \tag{1}$$

where $\delta(\ \ )$ denotes the change of $(\ \ )$ in response to the quadrupling of CO_2 content. S and F are the net downward solar radiation and upward terrestrial radiation at the top of the model atmosphere, respectively. δS and δF may be approximated as

$$\delta S \approx \delta_{CO_2}S + \delta_r S + \delta_A S + \delta_c S, \tag{2}$$

$$\delta F \approx \delta_{CO_2}F + \delta_T F + \delta_r F + \delta_c F, \tag{3}$$

where $\delta_x S$ and $\delta_x F$ denote the changes in S and F attributable to a change in a variable χ (i.e., δ_x) when it is assumed that all other relevant variables do not change. Here, the subscripts CO_2, T, r, A and C denote carbon dioxide content of air, atmospheric temperature, mixing ratio of water vapor, surface albedo and cloud cover, respectively.

The approximate expressions which are listed above, hold provided that the changes of these variables are small. The results of this analysis are presented in Table 3. From this table, it is seen that the major contributions to δR come from changes of temperature, water vapor and CO_2 content, while a lesser contribution comes from a change of surface albedo in high latitudes. Since both the standard and $4 \times CO_2$ atmospheres, are very close to radia-

tive equilibrium (i.e., $\overline{R}^A = 0$), the area mean value of δR (i.e., $\overline{\delta R^A}$) is equal to zero as the δY column of Table 3 indicates. However, $\overline{\delta R}^A$, which is computed from the approximate equations (1), (2) and (3), does not vanish because of the nonlinear interaction among the relevant variables as Table 3 indicates (the Σ column). It is of particular interest to note here that contributions $\delta_c S$ and $\delta_c F$ almost cancel out each other, which indicates the smallness of the net contribution of cloud feedback. In other words, the change in terrestrial radiation caused by the cloud change is compensated by the accompanying change in solar radiation.

Further analysis of the results shows that, equatorward of 50° latitude, the reductions of both total cloudiness and effective cloud-top height contribute to the increase in the effective emission temperature of the upward terrestrial radiation and enhance the cooling of the model atmosphere. On the other hand, the aforementioned reduction of cloud amount results in the decrease of the reflected solar radiation (or increase in net incoming solar radiation) and accordingly increases the absorption of solar radiation by the earth-atmosphere system of the model. Thus, the effect of the cloud-induced increase in outgoing terrestrial radiation almost compensates for the effect of the corresponding increase in net incoming solar radiation. Poleward of 50° latitude, cloudiness increases without significantly altering the effective cloud-top height. Since the incoming solar radiation is small in high latitudes, the heat loss due to the cloud-induced reduction of the net incoming solar radiation is almost compensated by the heat gain due to the corresponding reduction of outgoing terrestrial radiation despite the absence of a change of the effective cloud-top height. Because of the compensation in both latitudinal zones, the overall effect of the cloudiness change on the heat balance of the atmosphere-earth system of the model is relatively small.

In view of the uncertainty in the values of the optical cloud parameters and the crudeness of the cloud prediction scheme incorporated into the model, it is premature to conclude that the change of cloud cover has little effect on the sensitivity of climate. However, it may not have as large an effect as some of the earlier studies (Manabe and Wetherald, 1967; Schneider, 1972) imply because of the compensative mechanism discussed above. This subject will be dealt with in more detail in the aforementioned future publication.

9. Summary and conclusions

It is shown that the general warming and the increase of moisture content in the model atmosphere due to a CO_2 increase results in the reduction of the meridional temperature gradient in the lower model

troposphere because of 1) the poleward retreat of highly reflective snow cover and 2) the increase of the poleward transport of latent heat. The first effect is particularly important at very high latitudes and the second effect exerts a smaller but more uniform influence at all latitudes.

The increase in the poleward moisture transport has an important hydrologic implication. Owing to this increase, the change in the mean precipitation rate has a large latitudinal dependence although the evaporation rate tends to increase uniformly at all latitudes in response to an increase of CO_2. It is found that the enhanced penetration of moisture into high latitudes markedly increases precipitation there and shifts the midlatitude rainbelt poleward. Thus, the rate of runoff from the model continent increases significantly in high latitudes. On the other hand, the poleward shift of the midlatitude rainbelt results in the absence of a significant increase in the precipitation rate and the reduction of soil moisture over the model continent in a zonal belt centered around 42° latitude. In this zonal continental belt, the eddy kinetic energy decreases significantly and is partly responsible for the aforementioned absence of the increase in the precipitation rate. In the model subtropics, an increase of carbon dioxide in the model atmosphere intensifies the monsoonal precipitation along the east coast of the model continent which results from the increase of the northward moisture transport along the periphery of the oceanic anticyclone. It is important to recognize that the results described above are obtained from a climate model with an idealized geography free of mountains and without seasonal variation. Therefore, one should not take too literally the details of the geographical distribution of climate change indicated in this study. Nevertheless, these results suggest that the climatic effect of a CO_2 increase may be far from uniform and may have significant geographical variation.

It is of interest that the response of the model climate to a doubling (or quadrupling) of CO_2 content is very similar to the corresponding response to a 2% (or 4%) increase of the solar constant. Both responses include a general warming of the troposphere-earth system of the model and decreases of a similar magnitude in the meridional temperature gradient although the latitudinal distributions of the direct radiative effect of these two forcings are quite different. As pointed out in the beginning of the preceding paragraph, the general warming of the model atmosphere results in the poleward retreat of snow cover and enhanced transport of latent energy and causes the large reduction of the meridional temperature gradient of the model troposphere. This effect is found to dominate over the difference between the latitudinal distributions of the two radiative forcings.

The reduction of the meridional temperature gradient, which accompanies the general warming of the model atmosphere, may have a paleoclimatic implication. One can speculate that the small meridional temperature gradient in the warm climate of the Mesozoic era, which is indicated by geological records, was partly sustained by a similar mechanism, i.e., a large poleward transport of latent energy.

It is suggested that the increase of CO_2 content affects not only the time-mean state, but also the variability of the model climate. For example, the variance of temperature in the lower model troposphere decreases substantially in response to the CO_2 increase. The aforementioned reduction of the meridional temperature gradient appears to be responsible for not only the reduction of eddy kinetic energy, but also the reduction of the variance of temperature.

The model used for this study contains an interaction among cloud cover, radiation and dynamics, i.e., a cloud feedback mechanism. It is found that the cloud feedback mechanism of the model has little effect on the overall sensitivity of climate. Obviously, the magnitude of the effect depends on the specific choice of the optical cloud parameters (i.e., reflectivity and absorptivity) which are not known accurately. Nevertheless, the results from this study identify an interesting mechanism of compensation which tends to reduce the net effect of cloud cover on the sensitivity of climate.

A natural extension of this study is a sensitivity study using a joint mixed-layer ocean-atmosphere model with a global computational domain, realistic geography and a seasonal variation of insolation. The construction of such a model is in progress at the Geophysical Fluid Dynamics Laboratory of NOAA.

REFERENCES

Augustsson, T., and V. Ramanathan, 1977: A radiative-convective model study of the CO_2 climate problem. *J. Atmos. Sci.*, **34**, 448–451.

Held, I. M., 1978: The tropospheric lapse rate and climate sensitivity: Experiment with a two-level atmospheric model. *J. Atmos. Sci.*, **35**, 2083–2098.

London, J., 1957: A study of the atmospheric heat balance. Final Report, Contract AF19(122)-165, New York University, 99 pp. [Available from NOAA, Users Services Branch, D822, Library & Info. Services Div., 6009 Executive Blvd. WSC-4, Rockville, MD 20852].

Manabe, S., 1969: Climate and the ocean circulation: I. The atmospheric circulation and the hydrology of the earth's surface. *Mon. Wea. Rev.*, **97**, 739–774.

——, and R. F. Strickler, 1964: Thermal equilibrium of the atmosphere with a convective adjustment. *J. Atmos. Sci.*, **21**, 361–385.

——, and R. T. Wetherald, 1967: Thermal equilibrium of the atmosphere with a given distribution of relative humidity. *J. Atmos. Sci.*, **24**, 241–259.

——, and R. T. Wetherald, 1975: The effects of doubling the CO_2 concentration on the climate of a general circulation model. *J. Atmos. Sci.*, **32**, 3–15.

——, J. Smagorinsky and R. F. Strickler, 1965: Simulated climatology of a general circulation model with a hydrologic cycle. *Mon. Wea. Rev.*, **93**, 769–798.

——, K. Bryan and M. J. Spelman, 1975: A global ocean-atmosphere climate model. Part I. The atmospheric circulation. *J. Phys. Oceanogr.*, **5**, 3–29.

Phillips, N. A., 1957: A coordinate system having some special advantages for numerical forecasting. *J. Meteor.*, **14**, 184–185.

Ramanathan, V., and J. A. Coakley, Jr., 1978: Climate modeling through radiative-convective models. *Rev. Geophys. Space Phys.*, **16**, 465–689.

Roads, J. O., 1978: Numerical experiments on the sensitivity of an atmospheric hydrologic cycle to the equilibrium temperature. *J. Atmos. Sci.*, **35**, 753–773.

Rodgers, C. D., and C. D. Walshaw, 1966: The computation of infrared cooling rate in planetary atmospheres. *Quart. J. Roy. Meteor. Soc.*, **92**, 67–92.

Rasool, S. I., and S. H. Schneider, 1971: Atmospheric carbon dioxide and aerosols: Effects of large increases on global climate. *Science*, **173**, 138–141.

Schneider, S. H., 1972: Cloudiness as a global climate feedback mechanism: The effects on the radiation balance and surface temperature of variations in cloudiness. *J. Atmos. Sci.*, **29**, 1413–1422.

——, 1975: On the carbon dioxide-climate confusion. *J. Atmos. Sci.*, **32**, 2060–2066.

——, W. M. Washington and R. M. Chervin, 1978: Cloudiness as a climate feedback mechanism: Effects on cloud amounts of prescribed global and regional surface temperature changes in the NCAR GCM. *J. Atmos. Sci.*, **35**, 2207–2221.

Smagorinsky, J., S. Manabe and J. L. Holloway, Jr., 1965: Numerical results from a nine-level general circulation model of the atmosphere. *Mon. Wea. Rev.*, **93**, 728–768.

Stone, H. M., and S. Manabe, 1968: Comparison among various numerical models designed for computing infrared cooling. *Mon. Wea. Rev.*, **96**, 735–741.

Telegadas, K., and J. London, 1954: A physical model for the Northern Hemisphere troposphere for winter and summer. Sci. Rep. No. 1, Contract AF19(122)-165, Res. Div. College of Engineering New York University, 55 pp. [Available from NOAA, User Services Branch, D822, Library & Inf. Services Div., 6009 Executive Blvd. WDC-4, Rockville, MD 20852. Cat. No. M(055).N532S #1].

Wetherald, R. T., and S. Manabe, 1975: The effects of changing the solar constant on the climate of a general curculation model. *J. Atmos. Sci.*, **32**, 2044–2059.